A Deep Neural Network Based UAV-assisted Wireless Network

Ibrahem Mouhamad, Weijia Zhang

***Abstract*—In this paper, we present a dataset and a deep neural network model for predicting signal quality in an urban outdoor environment for Unmanned Aerial Vehicles (UAVs)-assisted wireless networks. The dataset contains Signal-to-Interference-plus-Noise Ratio (SINR) and Line-of-Sight (LoS) values for different locations and heights in the region of interest, calculated using a ray-tracing model based on the Shooting and Bouncing Rays (SBR) method. We analyze the dataset to investigate the dependence of SINR and LoS values on the distance and height of the receiver. We also propose a Deep Neural Network (DNN) model trained on the dataset to predict signal quality in the selected region at different heights. We evaluate the performance of the DNN model and show that it can accurately predict the coverage probability in the region of interest.**

***Keywords*—deep neural network, signal-to-interference-plus-noise ratio, dataset.**

I. Introduction

Smart cities, mobile networks, the Internet of Things, driverless cars, and many more applications and services are made possible by wireless communication, which is an essential technology [1–3]. Unmanned Aerial Vehicles (UAVs) have become a viable way to improve wireless network performance. UAVs are able to operate as wireless network providers as well as users [4,5]. By connecting remote or difficult-to-reach places, UAVs can enhance wireless networks' capacity, coverage, and energy efficiency in their role as providers [4]. Their flexibility, mobility, and adaptability make them well-suited for this role. As consumers, UAVs can utilize existing networks to support applications such as remote sensing, virtual reality, and item delivery [4].

However, wireless communication is subject to various factors that can affect its performance, including distance, height, frequency, interference, noise, weather conditions, and environmental geometry [6, 7]. The environment in which the signals are transmitted and the likelihood of line-of-sight between the UAV and ground station, which is dependent on the UAV's flying height [4], both affect the air-to-ground communication channel between the UAV and the ground station. It is therefore important to understand and model the wireless communication environment in order to optimize network performance and air-to-ground signal quality.

One approach to modeling the wireless communication environment is through the use of ray-tracing methods. These methods simulate the propagation of radio waves in a given environment by tracing the paths of rays that reflect and diffract from different surfaces and objects [8, 9]. Ray-tracing methods can provide accurate and realistic results but require detailed information about the environment's geometry and material properties as well as significant computational resources [9, 10].

Machine learning (ML) has the potential to revolutionize wireless networks by enabling more intelligent functions that optimize network operations and meet the diverse needs of emerging wireless applications [4]. With ML, wireless networks can proactively take more adequate actions by learning and predicting various factors such as traffic patterns, communication channel dynamics, user context, content requests, and more [4].

In this paper, we introduce a dataset of signal-to-interference-plus-noise ratio (SINR) and line-of-sight (LoS) values for wireless communication in an urban outdoor environment. We employ a ray-tracing model based on the Shooting and Bouncing Rays (SBR) method [11] to calculate signal propagation paths and losses between 18 ground base stations and a receiver at various locations and heights in a region of interest. We analyze the dataset to investigate the dependence of SINR and LoS values on the distance and height of the receiver. The simulation results provide insight into the propagation environment for the deployment of UAVs as providers or consumers of wireless networks. The dataset can be utilized for a range of applications, including the development and validation of propagation models, optimization of wireless network design, and investigation of environmental factors on wireless communication.

To address the computational costs associated with the SBR method [9, 10], we propose a deep neural network (DNN) model trained on the resulting dataset to predict signal quality in the selected region at different heights. This model can be used to optimize trajectory planning and placement of UAVs. Additionally, it can serve as a pre-trained model that can be fine-tuned by UAVs using their collected data.

II. System Model

The system consists of N transmitters located at different locations (x_n, y_n, z_n), where $n = 1, 2, \ldots, N$ in an outdoor environment. A single receiver is located at position (x_r, y_r, z_r) in the same outdoor environment. Each transmitter n at position (x_n, y_n, z_n) transmits signal of

Ibrahem Mouhamad - School of computer science and Robotics, Tomsk Polytechnic University, Tomsk, 634050, Russian Federation. (corresponding author) ORCID: 0000-0003-1569-5493 email: ibragim1@tpu.ru
Weijia Zhang - School of computer science and Robotics, Tomsk Polytechnic University, Tomsk, 634050, Russian Federation. ORCID: 0000-0003-2252-2750 email: victoryzh@tpu.ru

frequency f and power P_n that propagates through the environment and is received by the receiver. The received signal power S_n at the receiver due to the n^{th} transmitter can be expressed taking into account the propagation loss, antenna gains, and any interference and noise present in the system. Mathematically, the received signal power can be represented as follows:

$$S_n = P_n G_n(\theta_n, \phi_n) G_r(\theta_r, \phi_r) L_n \quad (1)$$

where $G_n(\theta_n, \phi_n)$ is the antenna gain of the n^{th} transmitter in the direction of (θ_n, ϕ_n), $G_r(\theta_r, \phi_r)$ is the antenna gain of the receiver in the direction of (θ_r, ϕ_r), θ_n and θ_r are the elevation angles, ϕ_n and ϕ_r are the azimuth angles, and L_n is the path loss between the n^{th} transmitter and the receiver. L_n depends on the propagation model and environment geometry. Fig. 1 shows an example with one receiver and two transmitters, along with the propagation paths between them.

Figure 1. The signal propagation paths between one receiver and two transmitters in a 3D environment

The interference power at the receiver due to all transmitters except the n^{th} transmitter is given by:

$$I = \sum_{m \neq n} I_m = \sum_{m \neq n} P_m G_m(\theta_m, \phi_m) G_r(\theta'_m, \phi'_m) L_m \quad (2)$$

where (θ'_m, ϕ'_m) are the angles of arrival of the interference signals at the receiver. The SINR at the receiver is given by:

$$SINR = \frac{S_n}{I + P_{noise}} \quad (3)$$

where P_{noise} is the noise power at the receiver.

For every transmitter-receiver pair, we must compute the route losses L_n and L_m in order to get the SINR at the receiver. This can be accomplished by either the image approach or the SBR method with a ray-tracing model [9, 11]. This model can be used to calculate propagation pathways with geometry from 3D environments [8] for frequencies between 100 MHz to 100 GHz [12]. To simulate radio wave propagation in a three-dimensional outside setting, the SBR approach is utilized. Free-space loss, reflection losses, and diffraction losses are taken into consideration in path loss computations [13]. The Fresnel equation, Uniform Theory of Diffraction (UTD) [14], geometric angle, and complex permittivity of interface materials ε_r [13] are used by the model to compute losses for each reflection and diffraction.

For a variety of frequencies, the ITU-R P.2040-2 [15] guidelines provide formulas, techniques, and numbers for calculating the ε_r of construction materials. ITU-R P.527-6 [16] contains the equations needed to compute complex permittivity values for Earth's surface. The following formula is used to compute the complex permittivity values for building materials ε_r [16]:

$$\varepsilon'_r = a f^b \quad (4)$$

$$\sigma = c f^d \quad (5)$$

$$\varepsilon_r = \varepsilon'_r + j \frac{\sigma}{2\pi \varepsilon_0 f} \quad (6)$$

where ε'_r is the relative permittivity, σ is the conductivity, ε_0 is the permittivity of free space, and f is the radio wave frequency. The constants a, b, c, and d are defined by the surface material.

III. Ray-tracing Simulations

A. Data Collection

To collect the dataset, a region of interest measuring 10x10 km was selected. To accurately model the impact of surrounding buildings on the propagation environment, OpenStreetMap (OSM) [17] was used to obtain a database of buildings in the region of interest. The OSM API was used to extract buildings data and incorporate it into the ray-tracing model to calculate SINR values. Fig. 2 shows the distribution of buildings inside the selected region, where approximately 40% of the area is occupied by buildings, while the remaining portion comprises terrain surface. The majority of building heights are lower than 10m.

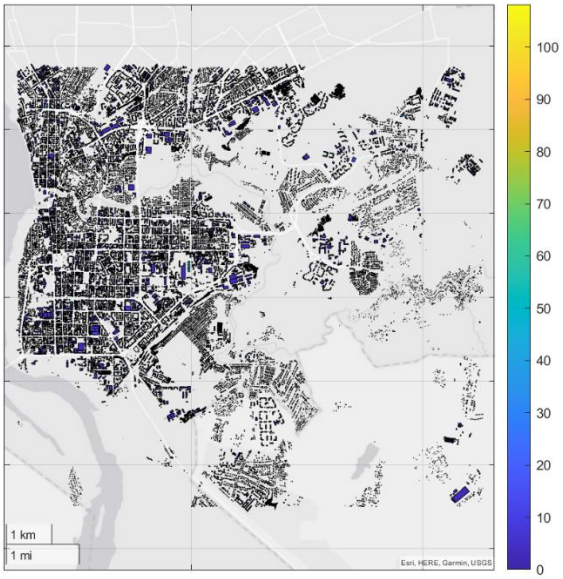

Figure 2. Buildings distribution in the selected region

A set of randomly selected points within the region of interest was generated, with the height of each point randomly chosen between 20m and 300m to capture the variation in SINR and the probability of LoS values. The SINR values were calculated for a receiver at each generated point and a set of transmitters, 18 ground base stations (GBs), located at specific points on the ground at a height of 10m with an operating frequency f of 2.5 GHz.

The ray-tracing model used the SBR method with a maximum of two reflections and one diffraction per ray. The model takes into account the position of ground base stations, surrounding buildings, building materials, and terrain materials to calculate signal strength and interference at each point.

The construction material is concrete, and the values $a = 5.31$, $b = 0$, $c = 0.0326$ and $d = 0.8095$ from Table 3 in [15] are used to calculate ε_r using (6), where $\varepsilon_r' = 5.31$ and $\sigma = 0.0684$ calculated using (4) and (5), respectively. The terrain material is vegetation, and ε_r is computed for temperatures above zero and utilizing formulas (51), (51), and (53) in [16].

In addition to SINR values, we also recorded LoS information for each ground base station and receiver pair. LoS information was calculated using a simple line-of-sight model that assumes a clear line-of-sight path between transmitter and receiver if there are no obstacles between them.

We use the Euclidean distance formula to calculate the distance $d_{i,r}$ between a receiver at location (x_r, y_r, h_r) and the transmitter i at location (x_i, y_i, h_i) in the UTM coordinate system [18], assuming negligible error due to the Earth's curvature at the scale of the selected region.

$$d_{i,r} = \sqrt{(x_r - x_i)^2 + (y_r - y_i)^2 + (h_r - h_i)^2} \qquad (7)$$

We compute the distance D_r between a receiver at location (x_r, y_r, h_r) and the N transmitters as follows:

$$D_r = \sum_{i=1}^{N} d_{i,r} \qquad (8)$$

We also compute the probability of LoS, $Prob_{LoS,r}$, for each data point (x_r, y_r, h_r) based on the LoS condition $LoS_{i,r}$ between each transmitter i and a receiver at that data point as follows:

$$Prob_{LOS,r} = \frac{\sum_{i=1}^{N} LOS_{i,r}}{N} \qquad (9)$$

B. Data Description

The dataset contains $8x10^4$ samples. Each sample consists of 24 dimensions: X coordinate, Y coordinate, height, SINR, LoS condition for each of the 18 transmitters, the propability of LoS using (9) and the distance using (8). The X and Y coordinates are defined in the Universal Transverse Mercator (UTM) coordinate system, which is easy to use and provides a constant distance relationship in meters anywhere on the map [18]. The height is measured in meters above the ground level and it varies from 20m to 300m. The LoS condition between each transmitter and a receiver at the point (X, Y) is recorded as a binary value, where 1 indicates a clear path and 0 indicates an obstructed path.

IV. Prediction of Signal Quality

Ray-tracing simulation give a good understanding of the propagation environment where the UAVs could be used for different use cases. However, the ray-trancing model with the SBR method are costly regarding the computational resources and the time needed to measure the signal quality at different locations in the area where the UAVs should operate [9,10]. To overcome these limitations, we use the collected dataset to train a deep neural network to help in prediction the signal quality in the region of interest.

A. Problem Formulation

The problem of predicting SINR at different locations can be formulated as follow: Let $D = \{(x_i, y_i, h_i, s_i)\}_{i=1}^{M}$ be a dataset containing M records. The vector (x_i, y_i, h_i) represents the 3D coordinates of the i^{th} point, while s_i is the SINR value. This can be done by a function $f: R^3 \rightarrow R$ that maps the input features to the output target (SINR) which is a regression problem. The SINR depends on many factors related to the propagation environments, thus, it is difficult to find a solution to this problem based only on a 3D coordinates. However, deep learning can be used to approximate the function f.

Let denote the approximation function $f_{\theta,i}(x_i, y_i, h_i) \approx s_i$ that is parameterized by the weights and biases θ of a neural network. The goal is to find θ that minimizes a loss function $L(\theta, f_\theta, s)$ [19]. $L(\theta, f_\theta, s)$ is used to measure the discrepancy between the predicted and true SINR values.

$$\min_{\theta} L(\theta, f_\theta, s) = \frac{1}{M} \sum_{i=1}^{M} L_i\left(\theta, f_{\theta,i}, s_i\right) \qquad (10)$$

SINR values are continuous and noisy, and may not have a simple relationship with the input features. Thus, this regression problem could be challenging. Therefore, we simplify it to a classification problem. In order to maintain a reliable connection between a UAV and its ground base station, it is necessary for the signal quality in the serving area to exceed a certain threshold, denoted by α. Therefore, we simplify the problem by discretizing the SINR values into two categories {0,1} based on the threshold α. Let us denote $g_i(s_i, \alpha)$ as follows:

$$g_i(s_i, \alpha) = \begin{cases} 1 & if \quad s_i \geq \alpha \\ 0 & if \quad s_i < \alpha \end{cases} \qquad (11)$$

Thus, $f_{\theta,i}$ can be rewritten as $f_{\theta,i}(x_i, y_i, h_i) \approx p_i$. p_i is a vector that indicates the probability of each category. Thus, the problem is now a classification problem and the cross-entropy can be used as a loss function. Thus, $L(\theta, f_\theta, s)$ can be defined as follows:

$$L(\theta, f_\theta, g) = -\frac{1}{M}\sum_{i=1}^{M}\left[g_i \log(p_{i,1}) + (1-g_i)log(1-p_{i,1})\right] \quad (12)$$

where $p_{i,1}$ is the probability of the i^{th} point belonging to the category 1.

B. *Proposed DNN Model*

As shown in Fig. 3, we suggest a DNN model that consists of an input layer, three hidden layers, and an output layer. H neurons are found in the first and third hidden layers, whereas $2H$ neurons are found in the second hidden layer. The output layer uses the Sigmoid activation function, whereas the hidden levels employ the ReLU activation function. After examining a number of structures with varying numbers of hidden layers, it was shown that the model's performance does not significantly improve when the number of hidden layers is increased above three.

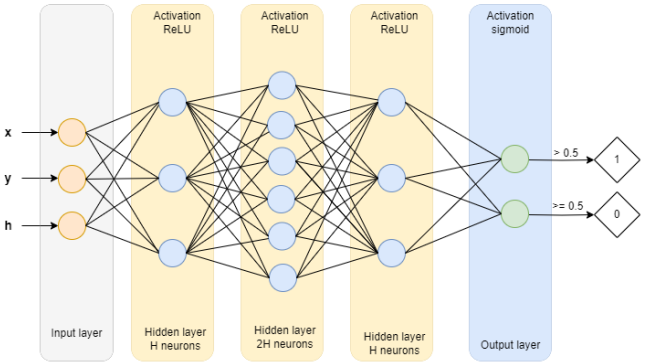

Figure 3. Deep neural network structure

C. *Data Prepossessing*

Normalizing the input data before feeding it into a neural network can help in ensuring that each feature contributes equally to the training process and can improve the convergence of the optimization algorithm [19]. The range normalization formula is defined as follows:

$$x_{norm} = \frac{x - x_{min}}{x_{max} - x_{min}} \quad (13)$$

where x is the original value of a feature, x_{min} and x_{max} are the minimum and maximum values of that feature, respectively, and x_{norm} is the normalized value of that feature. Equations (11) and (13) were used to normalize the values in the dataset before training. Moreover, the dataset was spitted into an 80\% training subset and a $20\% validation subset. The training subset was used to train the neural network, while the validation subset was used to evaluate the performance of the trained neural network on data that it had not seen during training.

V. RESULTS

A. *Exploratory Data Analysis*

In this section, we examine the dataset to learn about its properties and look for any trends or patterns. The histograms for the X and Y coordinates are displayed in Fig. 4 and Fig. 5, respectively. The data samples are not evenly distributed over the X and Y dimensions, but rather are more concentrated at some intervals than others, as the histograms show. However, we can notice that every interval has at least 200 samples. Thus, that there are no gaps or sparse areas in the data, which indicates that the data is relatively dense and covers a wide range of X and Y coordinates.

If we look at the height dimension, as Fig. 6 shown, we can confirm that the samples are densely distributed, with no intervals having zero or very few samples. Moreover, the samples do not have a distinct mode or peak in their heights.

The distribution of data samples along the SINR dimension is shown in Fig. 7. The tallest bar in the histogram indicates that the samples have a unimodal distribution with a mode of -5 dB. Additionally, the samples have a lengthy right tail in the histogram and are positively skewed. This implies that there are more samples with low SINR than with high SINR, and thus the data is lopsided.

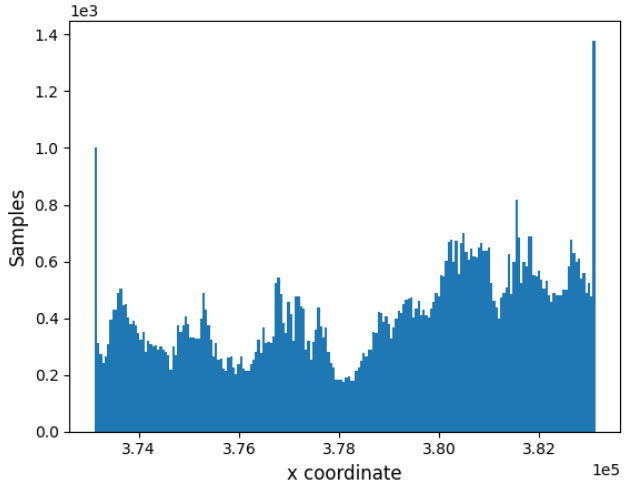

Figure 4. Samples distribution along the X coordinates

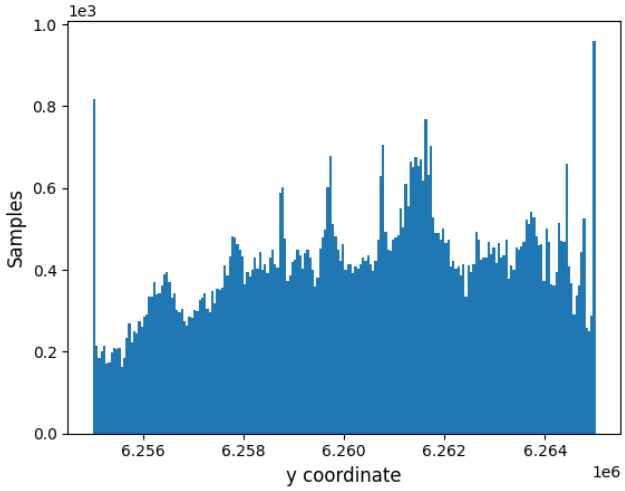

Figure 5. Samples distribution along the Y coordinates

The data sample distribution along the LoS dimension is displayed in Fig. 8. The majority of the transmitters have a large number of samples with a LoS value of 1, as the bar graph shows. This suggests that the non-LoS condition is rare among the samples and that LoS is not a significant or typical component of the data. Transmitter 11 alone, for example, has fewer than $2x10^4$ samples; the rest have more

than $4x10^4$ samples. This implies that in nearly every place within the chosen region, there is a high likelihood of having LoS between the receiver and the majority of the transmitters. However, because the majority of the samples have low SINR values, the signal quality is typically poor. This suggests that even with a high risk of loss of service, the signal quality is diminished by both environmental interference and signal attenuation as it spreads over a wide region.

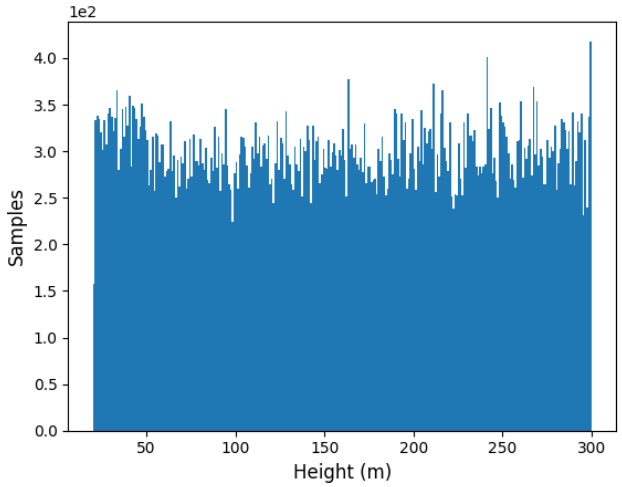

Figure 6. Samples distribution along the height dimension

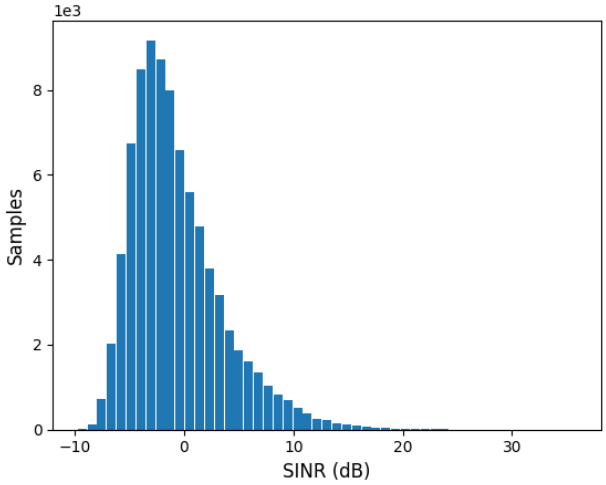

Figure 7. Samples distribution along the SINR dimension

Fig. 9 plots the SINR values versus the distance for different heights. We observe that the SINR values decrease as the distance between the receiver and the transmitter increases, irrespective of the height of the receiver. This implies that the signal quality deteriorates as the distance grows. However, we can also infer that the height of the receiver affects how quickly the SINR values decrease. The higher the receiver, the slower the decrease for heights from 50m to 200m.

The probability of LOS decreases as the distance between the receiver and transmitter increases, irrespective of height, as shown in Fig. 10. This implies that having a direct line of sight between them becomes less likely as they move farther apart. However, we can also infer that height affects how quickly this probability decreases. The higher the receiver, slower is this decrease for heights from 50m to 150m.

B. Deep Learning Model Architecture Selection

We tuned the hyperparameter H, which controls the number of neurons in the hidden layers of the proposed DNN model architecture, to optimize the model's performance. Fig. 11 (a) shows the loss function values for different values of H. The loss function decreases as H increases, indicating that the model becomes more accurate with more neurons in the hidden layers. Fig. 11 (b) shows the validation accuracy values for different values of H. The validation accuracy increases as H increases, until $H = 1024$, where it stagnates. This suggests that increasing H beyond a certain point does not improve the model's performance, but rather increases its computational cost and training time.

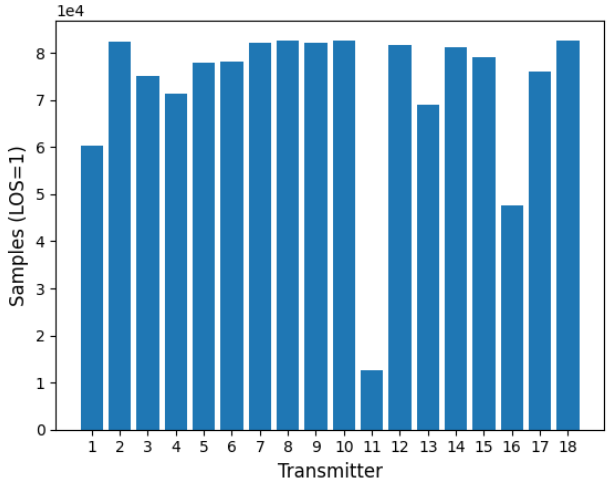

Figure 8. Samples distribution along the LOS dimension for each transmitter

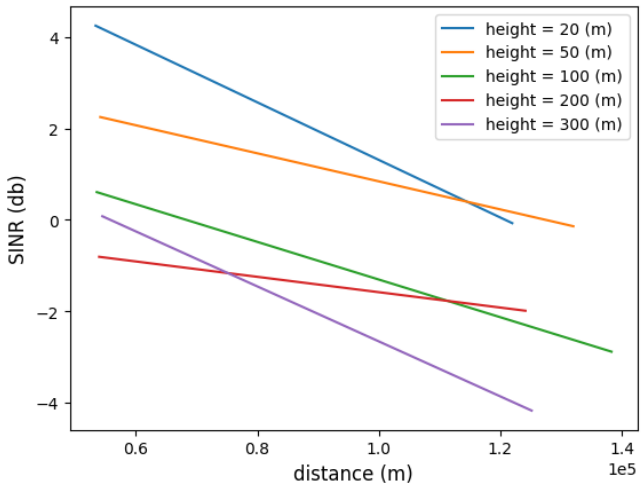

Figure 9. SINR values versus distance at different heights

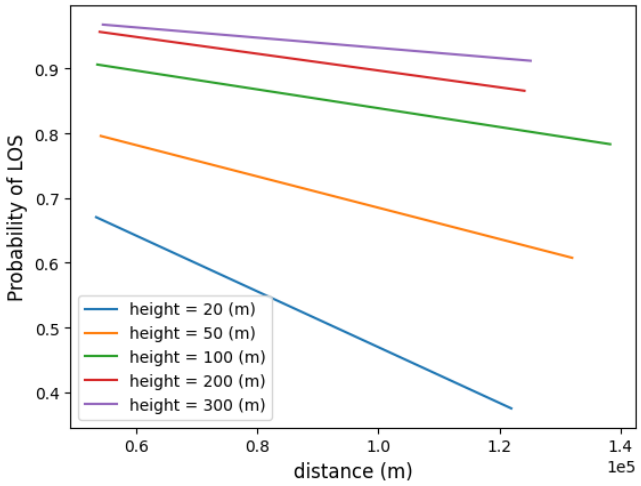

Figure 10. Probability of LOS versus distance at different heights

Moreover, we observe that for $H = 64$ and $H = 128$, the

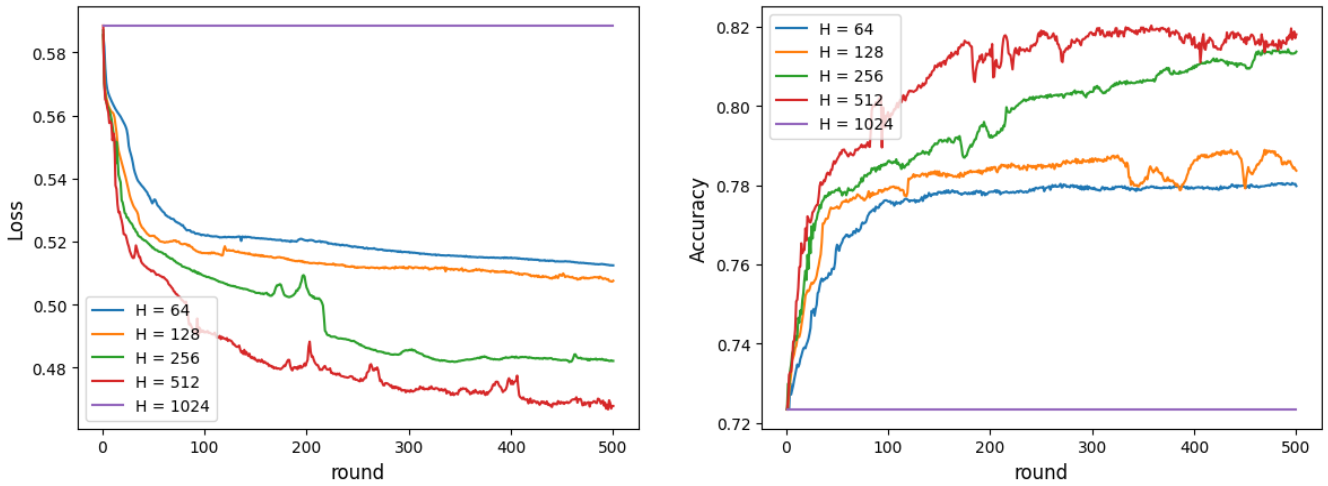

(a) (b)

Figure 11. Training results for different H values: a) training loss, b) validation accuracy

loss function plateaus after some training rounds, implying that the model has reached its optimal state and further training does not improve its predictive power. In fact, the validation accuracy decreases for $H = 128$, indicating that the model overfits the training data and fails to generalize to new data. For $H = 256$ and $H = 512$, the loss function and the validation accuracy continue to improve throughout the training process, suggesting that these values are more suitable for the model. However, since there is no significant difference between $H = 256$ and $H = 512$ in terms of performance, we choose $H = 256$ as the optimal value to balance model complexity and performance.

C. Signal Quality Predictions

We employed the DNN model to forecast the signal quality in the chosen area once it had been trained. Fig. 12 shows the coverage probability in the region of interest at different heights. It is seen that each ground base station's coverage area is predicted by the DNN model with accuracy. A center with a coverage probability of one exists in each of the coverage zones, and its coverage probability diminishes with distance. It's also important to remember that the coverage area decreases with height.

VI. Discussion

In this paper, we have presented a novel approach to model and predict the wireless communication environment for UAVs in an urban outdoor scenario. We have used a ray-tracing technique based on the SBR method to generate a dataset of SINR and LoS values for different locations and heights. We have analyzed the dataset to investigate the dependence of SINR and LoS values on the distance and height of the receiver. We have found that the SINR values decrease as the distance increases, irrespective of the height, while the LoS probability decreases as the distance increases, but is affected by the height. We have also found that the signal quality is generally poor, despite the high LoS probability, due to the interference and attenuation effects of the environment.

We have presented a DNN model trained on the generated dataset to forecast signal quality in the targeted region at different heights, hence mitigating the computational costs associated with the SBR technique. After fine-tuning the DNN model's hyperparameters to maximize performance, we assessed the accuracy of the model on a validation subset. We have demonstrated that the coverage probability in the region of interest corresponding to each ground base station can be reliably predicted by the DNN model. Additionally, we have demonstrated that when height increases, the coverage area reduces.

Our method has a number of benefits. First, by

accounting for the geometry and material properties of the 3D environment, it can produce results that are accurate and lifelike. Second, by employing a DNN model trained on a ray-tracing dataset, it can cut down on both computational complexity and time. Thirdly, by altering the ray-tracing model's input parameters and retraining the DNN model, it is readily adjustable to various circumstances and frequency.

Future research must address the limitations and difficulties of our approach. Initially, our dataset is restricted to a single area and frequency range. Second, the static dataset used to train our DNN model ignores dynamic elements like traffic, weather, movement, and outside interference. It would be useful to incorporate these factors into our dataset and DNN model to make them more robust and adaptive.

VII. Conclusion

In conclusion, we provided a dataset of SINR and LoS values for outdoor wireless communication, which were determined using a ray-tracing model derived from the SBR technique. The model considers how adjacent buildings affect the environment for wireless communication. The dataset can be applied to a number of tasks, including wireless network design optimization and the creation and validation of propagation models. We suggested a DNN model trained on the dataset to forecast signal quality in the targeted region at different heights in order to mitigate the computational expenses related to the SBR method. Without the need for laborious and time-consuming ray-tracing simulations, the DNN model can provide quick and accurate predictions and is easily customizable to account for variations in the surrounding environment. We plan to use the DNN model as

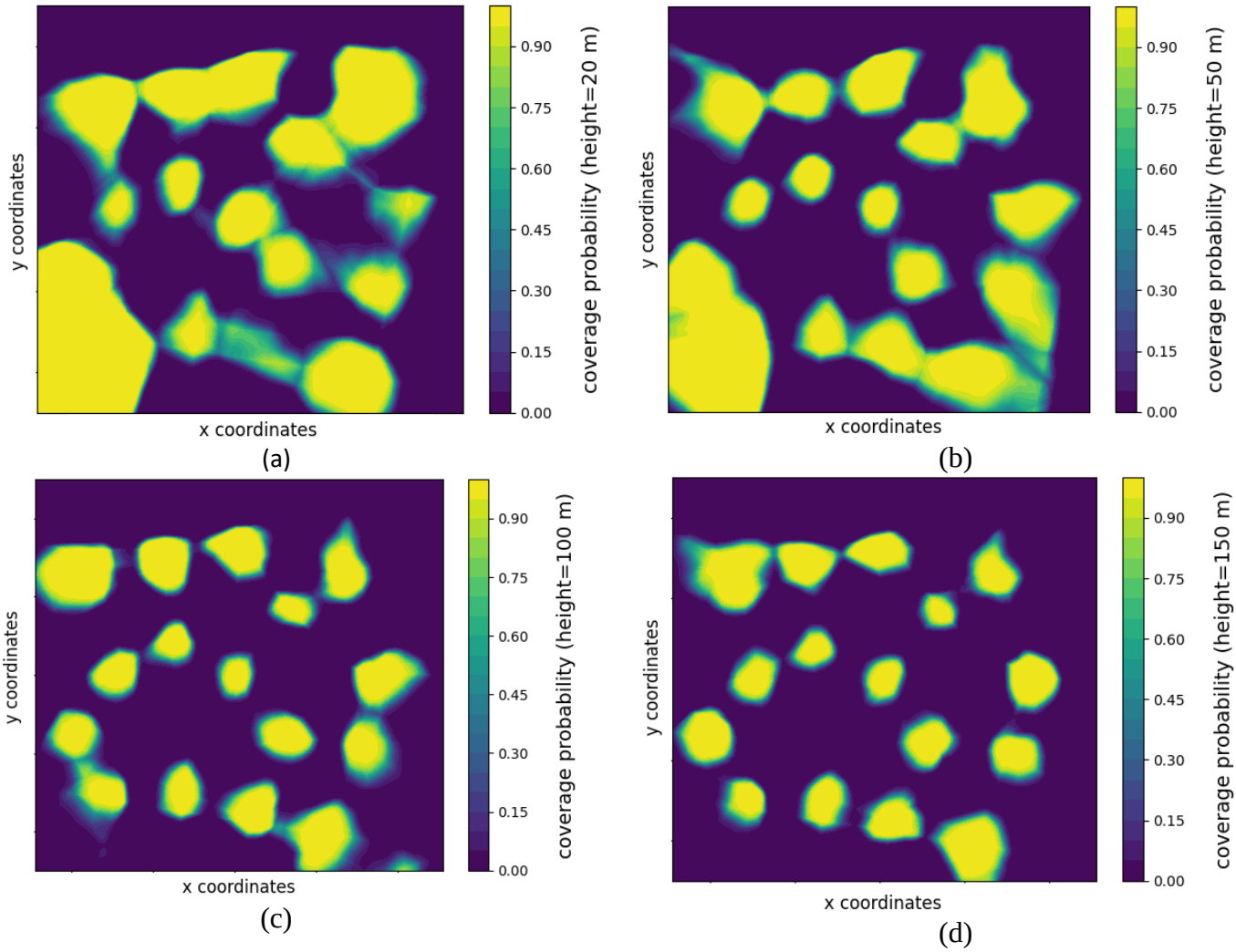

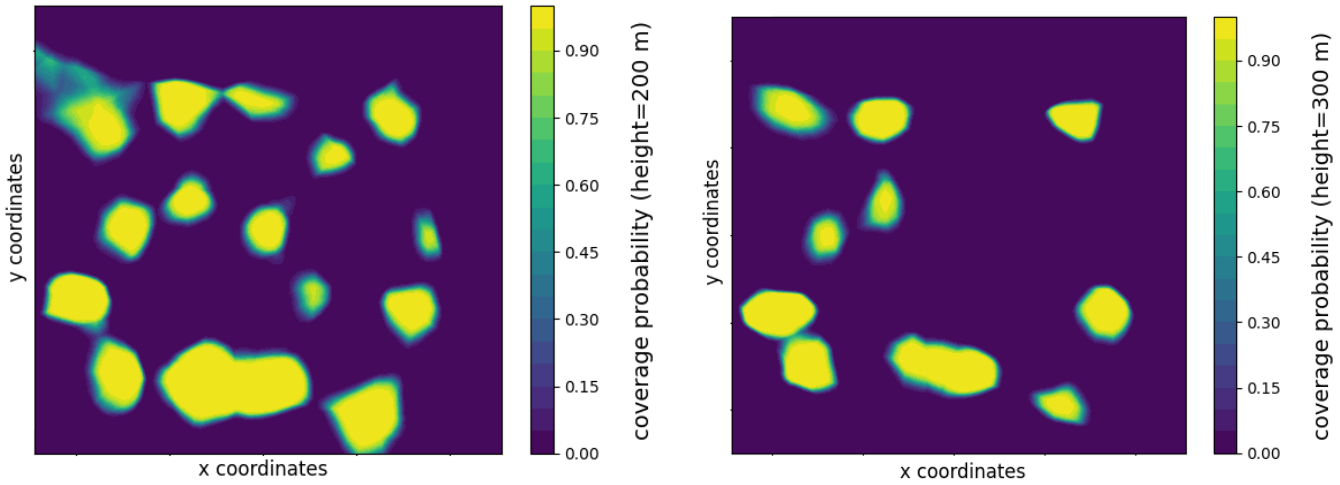

Figure 12. Predicted coverage probability in the region of interest at different altitudes: a) 20m, b) 50m, c) 100m, d) 150m, e) 200m, f) 300m.

a pre-trained model that can be fine-tuned by UAVs using their collected data.

REFERENCES

[1] M. Z. Chowdhury, M. Shahjalal, S. Ahmed, and Y. M. Jang, "6G Wireless Communication Systems: Applications, Requirements, Technologies, Challenges, and Research Directions," IEEE Open Journal of the Communications Society, vol. 1, pp. 957–975, 2020, conference Name: IEEE Open Journal of the Communications Society.

[2] Q. V. Khanh, N. V. Hoai, L. D. Manh, A. N. Le, and G. Jeon, "Wireless Communication Technologies for IoT in 5G: Vision, Applications, and Challenges," Wireless Communications and Mobile Computing, vol. 2022, p. e3229294, Feb. 2022, publisher: Hindawi. [Online]. Available: https://www.hindawi.com/journals/wcmc/2022/3229294/

[3] M. F. Ali, D. N. K. Jayakody, S. Garg, G. Kaddoum, and M. S. Hossain, "Dual-hop mixed fso-vlc underwater wireless communication link," IEEE Transactions on Network and Service Management, vol. 19, no. 3, pp. 3105–3120, 2022.

[4] B. Brik, A. Ksentini, and M. Bouaziz, "Federated Learning for UAVs-Enabled Wireless Networks: Use Cases, Challenges, and Open Problems," IEEE Access, vol. 8, pp. 53 841–53 849, 2020, conference Name: IEEE Access.

[5] M. Mozaffari, W. Saad, M. Bennis, Y.-H. Nam, and M. Debbah, "A Tutorial on UAVs for Wireless Networks: Applications, Challenges, and Open Problems," Mar. 2019, arXiv:1803.00680 [cs, math]. [Online]. Available: http://arxiv.org/abs/1803.00680

[6] D. Tse and P. Viswanath, Fundamentals of Wireless Communication, illustrated edition ed. Cambridge, UK ; New York: Cambridge University Press, Jul. 2005.

[7] M. F. Ali, D. N. K. Jayakody, and Y. Li, "Recent trends in underwater visible light communication (uvlc) systems," IEEE Access, vol. 10, pp. 22 169–22 225, 2022.

[8] K. Schaubach, N. Davis, and T. Rappaport, "A ray tracing method for predicting path loss and delay spread in microcellular environments," in [1992 Proceedings] Vehicular Technology Society 42nd VTS Conference - Frontiers of Technology, May 1992, pp. 932–935 vol.2, iSSN: 1090-3038.

[9] Z. Yun and M. F. Iskander, "Ray Tracing for Radio Propagation Modeling: Principles and Applications," IEEE Access, vol. 3, pp. 1089–1100, 2015, conference Name: IEEE Access.

[10] D. Shi, X. Tang, and C. Wang, "The acceleration of the shooting and bouncing ray tracing method on GPUs," in 2017 XXXII-nd General Assembly and Scientific Symposium of the International Union of Radio Science (URSI GASS), Aug. 2017, pp. 1–3.

[11] H. Ling, R.-C. Chou, and S.-W. Lee, "Shooting and bouncing rays: calculating the RCS of an arbitrarily shaped cavity," IEEE Transactions on Antennas and Propagation, vol. 37, no. 2, pp. 194–205, Feb. 1989, conference Name: IEEE Transactions on Antennas and Propagation.

[12] International Telecommunications Union Radiocommunication Sector, "Propagation data and prediction methods for the planning of short-range outdoor radio-communication systems and radio local area networks in the frequency range 300 MHz to 100 GHz," Recommendation P.1411-11. ITU-R, 2021.

[13] T. M. Inc., "Ray tracing propagation model," Natick, Massachusetts, United States, 2023. [Online]. Available: https://www.mathworks.com/help/stats/index.html

[14] D. A. McNamara and C. W. I. Pistotius, Introduction to the Uniform Geometrical Theory of Diffraction, illustrated edition ed. Boston: Artech Print on Demand, Jan. 1990.

[15] I. T. U. R. Sector, "Effects of building materials and structures on radio wave propagation above about 100 mhz," Recommendation P. 2040-2. ITU-R, 2021.

[16] International Telecommunications Union Radiocommunication Sector, "Electrical characteristics of the surface of the Earth," Recommendation P. 527-6. ITU-R, 2021.

[17] "OpenStreetMap." [Online]. Available: https://www.openstreetmap.org/

[18] "The Universal Transverse Mercator (UTM) Grid," USGS Publications Ware-house, 2001.

[19] R. Sun, "Optimization for deep learning: theory and algorithms," Dec. 2019, arXiv:1912.08957 [cs, math, stat]. [Online]. Available: http://arxiv.org/abs/1912.08957.